Self-irradiation damage to the local structure of plutonium and plutonium intermetallics

C. H. Booth,[1] Yu Jiang,[1] S. A. Medling,[1] D. L. Wang,[2] A. L. Costello,[3] D. S. Schwartz,[3] J. N. Mitchell,[3] P. H. Tobash,[3] E. D. Bauer,[4] S. K. McCall,[5] M. A. Wall,[5] and P. G. Allen[5]
[1]*Chemical Sciences Division, Lawrence Berkeley National Laboratory, Berkeley, California 94720, USA*
[2]*Nuclear Sciences Division, Lawrence Berkeley National Laboratory, Berkeley, California 94720, USA*
[3]*Materials Science and Technology Division, Los Alamos National Laboratory, Los Alamos, New Mexico 87545, USA*
[4]*Materials Physics and Applications Division, Los Alamos National Laboratory, Los Alamos, New Mexico 87545, USA*
[5]*Condensed Matter and Materials Division, Lawrence Livermore National Laboratory, Livermore, California 94550, USA*

(Received 29 November 2012; accepted 18 February 2013; published online 4 March 2013)

The effect of self-irradiation damage on the local structure of δ-Pu, $PuAl_2$, $PuGa_3$, and other Pu intermetallics has been determined for samples stored at room temperature using the extended x-ray absorption fine-structure (EXAFS) technique. These measurements indicate that the intermetallic samples damage at a similar rate as indicated in previous studies of $PuCoGa_5$. In contrast, δ-Pu data indicate a much slower damage accumulation rate. To explore the effect of storage temperature and possible room temperature annealing effects, we also collected EXAFS data on a δ-Pu sample that was held at less than 32 K for a two month period. This sample damaged much more quickly. In addition, the measurable damage was annealed out at above only 135 K. Data from samples of δ-Pu with different Ga concentrations and results on all samples collected from different absorption edges are also reported. These results are discussed in terms of the vibrational properties of the materials and the role of Ga in δ-Pu as a network former. © *2013 American Institute of Physics*. [http://dx.doi.org/10.1063/1.4794016]

I. INTRODUCTION

Self-irradiation damage occurs in materials containing radioactive isotopes, and is responsible for a variety of phenomena, both in natural materials (metamict materials) and in man-made materials involving nuclear power and the nuclear-weapons stockpile. Although the subject has been studied extensively since the late 1940s, a microscopic level of understanding has not been achieved, especially in elemental plutonium. For instance, although the theories of defect production[1,2] and lattice relaxation[3,4] have been well developed, sub-Angstrom-level structural probes have not been suitably employed to verify these theories. Such verification is especially important for plutonium-bearing materials, since the *f*-orbitals possess extended bonding characteristics,[5] raising the possibility that correlated electron effects may play a role not only in determining magnetic and electronic properties[6] but also in how the material responds structurally to damage cascade events. Here, experiments are reported that represent a step toward understanding self-irradiation damage in plutonium-bearing materials by examining the changes in the local structure of a small range of Pu compounds ($PuAl_2$,[7] $PuGa_3$,[8] $PuCoGa_5$,[9] $PuCoIn_5$,[10] $PuPt_2In_7$,[11] and Pu_2PtGa_8) and in δ-Pu, both as a function of composition and as a function of storage temperature.

Self-irradiation damage in Pu-bearing materials occurs after an element in the material undergoes radioactive decay. Nearly all the damage is caused by the U recoil nucleus from α-decay of a Pu atom. For instance, a billiard-ball model of self-irradiation damage in δ-Pu indicates that for a ^{239}Pu atom decaying into a 5 MeV α particle and an 86 keV ^{235}U recoil nucleus, the α-particle generates about 265 Frenkel pairs (interstitials + vacancies), while the U nucleus generates 2290 Frenkel pairs over a distance of about 12 nm.[12] As will be discussed below, these numbers vary drastically in molecular dynamics calculations, especially as a function of time and temperature.

Previous local structure studies of related systems point to deficiencies in the current microscopic models, especially with regard to the apparent defect production rate and the effect of local distortions. For instance, magic-angle nuclear magnetic resonance studies of ^{239}Pu-spiked natural zircons indicate defect production rate up to a factor of 5 higher than predicted by simple theory.[13] The magnetic susceptibility of aged δ-Pu material indicates a weakly forming magnetic component,[14] allowing for a measure of the volume of damaged material per decay event. Surprisingly, this volume was a factor of 100 larger than the predicted volume of a damage cascade.[14] Extended x-ray-absorption fine-structure (EXAFS) measurements on $PuCoGa_5$ have also indicated a faster rate of damage, with about a factor of 10 more atoms involved in each damaging α-decay event than predicted from the expected defect production rate.[15,16] A unifying theme of all of these results is the importance of the dominating role of lattice distortions around Frenkel defect pairs as the driving force that determines the radiation-damaged-induced properties of these materials.

The presentation of the results on the intermetallic compounds and the δ-Pu samples begins with a description of the

sample preparation and analytical methods in Sec. II. The experimental results are presented in detail in Sec. III. Section IV discusses the results, focussing on qualitative and quantitative characteristics of the measured damage as it relates to vibrational properties, especially considering annealing effects.

II. EXPERIMENTAL METHODS

The isotopic content of the different samples varies slightly, but is about 94% ^{239}Pu and 6% ^{240}Pu, with small amounts of ^{238}Pu, ^{240}Pu, and ^{242}Pu, as well as ^{241}Am.

All intermetallic compounds were synthesized using previously published methods.[17]

The 1.9 at. % and 4.3 at. % Ga δ-Pu samples were prepared from electrorefined material and annealed in a vacuum furnace for 72 h at 440 °C. The estimated variation of Ga was about ±0.2 at. % within a typical 25 μm grain-size diameter. The 1.9 at. % and 4.3 at. % Ga δ-Pu samples were prepared by roughly lapping using a finer succession of diamond lapping film (30, 9, 3, and 1 μm) on both sides to a final thickness of ~90 μm. The final polish was a combination of 1 μm diamond paste on nylon and a final electropolish using a 10% nitric acid, 45% ethanol, 45% butoxyethanol solution at −15 °C for 20 s and 125 V DC. This last step is to remove any residual damage from the mechanical polishing. The final thickness of the specimens was ~80 μm. The samples were then dip-coated in liquid Kapton and cured at 150 °C for 4 h. The thickness of the Kapton when cured is ~10 μm. This final heat treatment should have removed any residual specimen preparation and radiation damage. All of these steps were performed in a dry N_2 or Ar atmosphere glovebox with a residual O_2 and H_2O of <10 ppm.

The 7 at. % Ga δ-Pu sample was made by melting electrorefined α-Pu with appropriate amounts of Ga in a crucible and subsequently casting into rods. One rod was annealed at 525 °C for ~100 h to uniformly distribute the Ga throughout the specimen. Ga concentration varied by 0.07 at. %, as determined by electron microprobe analysis. The grain diameter was ~50 μm. A small portion of this rod was removed with a slow speed diamond saw and lapped on silicon carbide grinding paper to ~150 μm.

Each sample was mounted in triply nested aluminum slotted holders with epoxy and indium sealed Kapton windows. The primary (inner) holder was sealed using dry N_2 gas around the 1.9 and 4.3 at. % Ga specimens, and dry laboratory air around the 7 at. % Ga specimen. Each sample was shipped to and measured at the Stanford Synchrotron Radiation Lightsource (SSRL). The reported sample ages in the data that follow are since the time of synthesis or the last damage-removing anneal.

It is important to note that the synthesis and safety requirements inherent in producing these materials were such that creating a collection of samples with identical ages was impossible, and in some cases, the amount of time from a sample's synthesis or last damage-removing anneal was fairly significant. For instance, some samples could not be measured for about 6 months (see Figs. 1 and 2). However, also note that for these samples, the age at first measurement as measured by the number of α-decays per atom remains

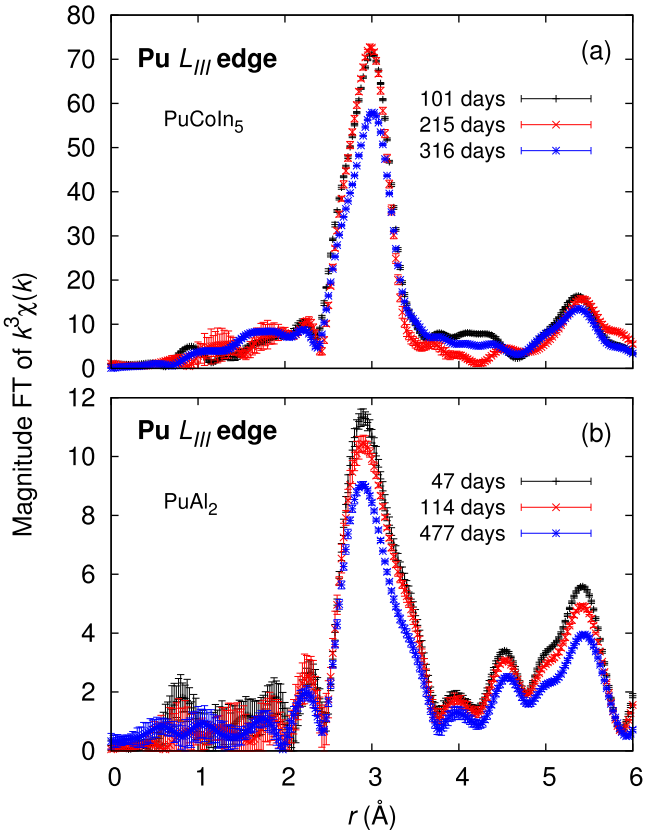

FIG. 1. FTs of $k^3\chi(k)$ from Pu L_3-edge data for (a) $PuAl_2$ and (b) $PuCoIn_5$. Transforms are from 2.5 to 14.0 Å^{-1}, Gaussian narrowed by 0.3 Å^{-1}.

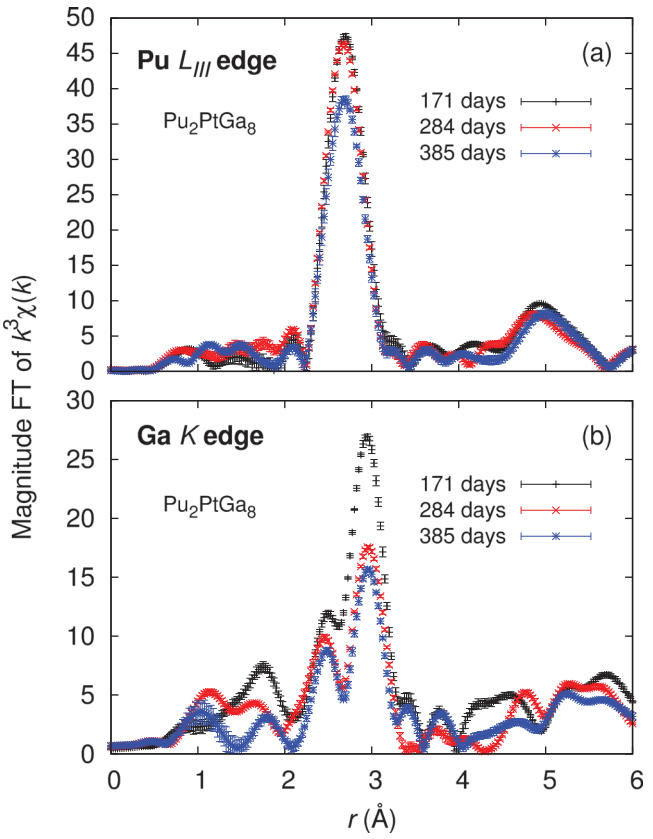

FIG. 2. FT magnitudes for Pu_2PtGa_8 from (a) Pu L_3-edge and (b) Ga K-edge data. Transforms are from 2.5 to 14.0 Å^{-1} for the Pu L_3-edge data, and from 2.5 to 13.9 Å^{-1} for the Ga K-edge data, each Gaussian narrowed by 0.3 Å^{-1}.

relatively low due to the relative number of Pu atoms per formula unit.

Data were collected over a period of several years at SSRL using a double-crystal Si(220) ($\phi = 0°$) monochromator, detuned by 50% to remove unwanted harmonic contamination. The data were collected on beam lines 11-2 and 10-2. Most samples are single polycrystals of material, too thick to collect data in transmission mode. For these samples, fluorescence-mode data were obtained using a 30-element Ge detector. Deadtime and self-absorption corrections were applied for all EXAFS data.[18] Data on $PuCoGa_5$, $PuGa_3$, and $PuAl_3$ were collected in transmission mode. These samples were ground and passed through a 30 μm sieve. The $PuAl_2$ sample was brushed onto clear adhesive tape and cut into strips which were subsequently stacked to achieve a change in the measured absorption edge of $\Delta\mu t \approx 1$, where μ is the absorption coefficient and t is the effective sample thickness. The other ground samples were mixed with boron nitride as a diluent and packed into an aluminum-slotted sample holder with a sample mass chosen such that $\Delta\mu t \approx 1$. The EXAFS oscillations were isolated from the total absorption using standard procedures.[19] In particular, a constant (for fluorescence data) or the result of a fit to a Victoreen formula (for transmission) was subtracted based on the pre-edge absorption, and an embedded-atom absorption, μ_0, was estimated by passing a cubic spline function through the data above the edge, typically between 4 and 7 knots. The EXAFS oscillations, $\chi(k)$, were then defined as $\chi(k) = \mu(k)/\mu_0(k) - 1$, where k is the photoelectron wavevector defined from $E - E_0 = \frac{\hbar^2 k^2}{2m_e}$, E is the incident photon energy, E_0 is chosen arbitrarily as the energy at the half-height of the absorption edge, and m_e is the rest mass of the electron. Data reduction otherwise utilized standard procedures using the RSXAP analysis codes[20,21] and backscattering amplitudes and phases calculated with the FEFF8 code.[22] Fits were performed in r-space, typically generating a backscattering amplitude, A, pair distance, r, and a pair-distance distribution variance σ^2 for each scatter path. A single amplitude reduction factor, S_0^2, is used for each fit as indicated, as well as a single threshold energy shift, ΔE_0. The number of neighbors, N, in a given scattering shell, i, is then given by $N_i = A_i/S_0^2$.

Damage fractions are determined from fits to the nominal crystal structure in a similar manner to previous work,[15,16] considering the loss of amplitude as due to a strongly damaged region. This method is straightforward and corresponds roughly to the number of atoms in a sample distorted by more than about 0.15 Å, based on our previous measurements on $PuCoGa_5$.[15,16] Specifically, if one assumes a displaced atom is strongly enough displaced (randomly over several tens of Angstroms), then the backscattering signal will average to zero. In this case, the only remaining amplitude is due to the undamaged fraction of the material; therefore, the damaged fraction is given by $F_d(t) = 1.0 - A(t)/A(0)$. If $A(t)$ has a non-zero contribution from damaged material, that is, the damaged-area contribution to $A(t)$ is not zero, then this estimate of $F_d(t)$ will be too small; that is, areas of the sample experiencing relatively small distortions will be counted as undamaged, yet may still contribute to changes in the material's electronic or magnetic properties.

III. RESULTS

A. Intermetallic compounds

Several intermetallic compounds were measured as a function of age, all stored at RT. In particular, $PuGa_3$, $PuAl_2$, $PuCoIn_5$, Pu_2PtGa_8, $PuPt_2In_7$, and two samples of $PuCoGa_5$ were measured, with some of the results on the $PuCoGa_5$ samples reported previously.[15,16] Representative EXAFS Fourier transforms (FTs) of $k^3\chi(k)$ are shown in Figs. 1 and 2. EXAFS FTs are similar to a radial partial pair distribution function, and as such, peaks in the FTs correspond to local structure features. The first peak in a FT is due to the nearest-neighbor photoelectron scattering from the absorbing atom. In the case of $PuAl_2$, the first peak corresponds to 12 Pu-Al nearest neighbor pairs at 3.25 Å and 4 Pu-Pu at 3.39 Å,[7] and for $PuCoIn_5$, the first peak corresponds to the combination of 8 Pu-In pairs at 3.23 Å and 4 Pu-In pairs at 3.26 Å.[10] The EXAFS FTs are not, however, actual distribution functions, since the scattering probabilities have both a real and imaginary components. Detailed fits are necessary to carefully extract structural information, although the fit results reported here only consider the nearest neighbors, greatly simplifying the analysis.

Fits to these data utilized the nominal crystal structures.[23] The derived damage fractions are reported in Fig. 3, which summarizes many of the results from this report. We note that not all the results from this work are shown in the figure for the sake of clarity; especially, the data from other edges are not all shown, although some of such results are reported in the other figures.

B. δ-Pu

When investigating structural issues in δ-Pu, microstructural features, such as grain boundaries, dislocations, precipitates, solute fractions, and surfaces, can play an important

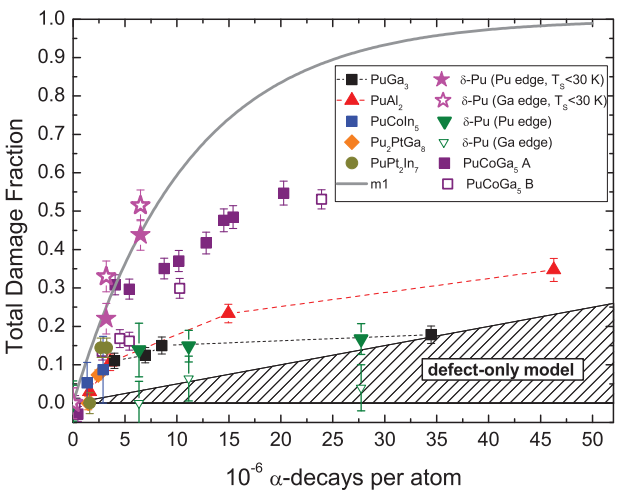

FIG. 3. Self-irradiation-induced damage fractions (F_d) measured from the Pu L_3 edge for samples stored at room temperature (T_S = RT), unless otherwise noted. Connecting lines for the $PuGa_3$ and $PuAl_2$ data are only guides to the eye. The solid gray line shows model "m1," Eq. (1) with 90 000 distortions per decay and the annealing rate constant $K = 0$. Note that the $T_S < 32$ K data are from a sample with 4.3 at. % Ga, while the T_S = RT data are from a 1.9 at. % Ga sample. The 4.3 at. % Ga sample also has some intrinsic disorder; see text for more information.

role, and may, in fact, determine certain features of the radiation-damage kinetics. Here, we are using the EXAFS technique to measure the result of such kinetics in terms of the average disorder (or distortion) per Pu or Ga atom. While microstructural features typically exist on length scales that are 100 or 1000 times greater than the regions that are part of a damage cascade, they are inherently low dimensional, and make up only a small fraction of the bulk material. Therefore, the EXAFS measurements reported below are only weakly sensitive to such effects.

We consider three issues that come into play when determining damage effects in δ-Pu: chemical composition, the role of annealing at room temperature, and the annealing-independent defect production rate. The local structure of δ-Pu is quite complex for a nominally *fcc* material, given the role of Ga concentration and possible intrinsic impurity phases that can exist. These features are important for understanding radiation damage effects, and so we begin by reporting the local structure results in some detail.

The *fcc* δ-phase of Pu is not the stable state at or below room temperature. A small amount of Ga (or other elements, including Am and Al) can be substituted into a Pu matrix to stabilize the *fcc* phase. Although the *fcc* phase is stabilized, such samples can be significantly disordered. As has been shown previously, the nearest-neighbor Ga-Pu pair distance is about 0.14 Å shorter than its Pu-Pu counterpart.[25–30]

Fit results to data collected on the 1.9 at. % Ga sample are reported in Fig. 4 and Table I, and are consistent with a well-ordered sample.[23] The temperature dependence of the Debye-Waller factors, $\sigma^2(T)$ are indicated from fits to the correlated-Debye model,[31,32] which is determined by a correlated-Debye temperature, Θ_{cD}, and a static offset, σ^2_{stat}. Usually, σ^2_{stat} is used to determine static disorder in a system, and can be used on the Pu L_3-edge data here. However, the pre-edge subtraction of the Ga *K*-edge data was affected by contamination of the Ga K_α fluorescence line by a large Compton peak contribution, which is likely the cause of the enhanced (>1) S_0^2 factor. Since S_0^2 is correlated with σ^2, we do not take the somewhat enhanced value of σ^2_{stat} for the Ga *K*-edge results as evidence of disorder around Ga in this material.

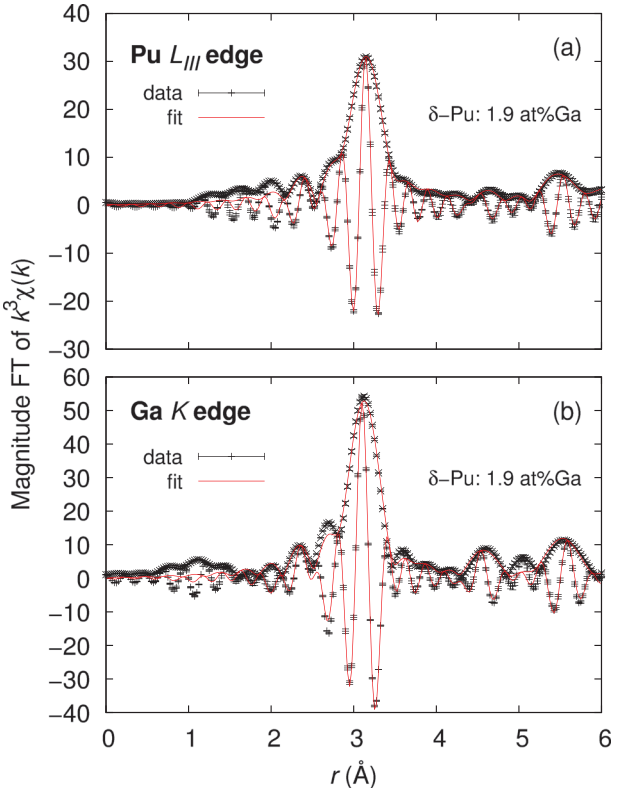

FIG. 4. FTs of $k^3\chi(k)$ data and fit results for 30 K data on δ-Pu: 1.9 at. % Ga, from both (a) the Pu L_3 edge and (b) the Ga *K* edge. The first peak at ~3.1 Å contains the signal from the 12 nearest neighbor Pu-Pu pairs in the *fcc* structure at 3.25 Å, as well as the 1.9% Ga contributions. Transform ranges are as given in Fig. 2.

TABLE I. Fit results from δ-Pu:1.9 at. % Ga data collected at 30 K. Fit range is between 2.5 and 6.6 Å, including all single-scattering paths as reported, as well as multiple scatter paths. The k^3-weighted Pu L_3-edge data are transformed between 2.5 and 14.0 Å^{-1}, and the Ga *K*-edge data are transformed between 2.5 and 13.9 Å^{-1}, each Gaussian narrowed by 0.3 Å^{-1}. The correlated-Debye fit results are from data collected at 30, 100, 200, and 300 K, and are only obtained from the σ^2s of the nearest-neighbor at 3.27 Å. Reported errors are determined using a Monte Carlo method[24] and primarily reflect reproducibility. Absolute errors for σ^2 are about 10% for near neighbors and 20% for further neighbors, and for *R* are about 0.005 Å for near neighbors and 0.02 Å for further neighbors.[19]

		Pu L_3 edge		Ga *K* edge	
	N	σ^2(Å^2)	*R*(Å)	σ^2(Å^2)	*R*(Å)
Pu(Ga)-Pu1	12	0.0030(1)	3.270(1)	0.0044(3)	3.134(3)
Pu(Ga)-Pu2	6	0.0059(5)	4.630(6)	0.007(1)	4.55(1)
Pu(Ga)-Pu3	24	0.0041(5)	5.643(5)	0.008(1)	5.60(1)
Pu(Ga)-Pu4	12	0.000(2)	6.56(1)	0.005(2)	6.62(2)
ΔE_0		1.8(3)		9.3(7)	
S_0^2		0.85(3)		1.1(1)	
Θ_{cD}		127(2)		212(5)	
σ^2_{stat}		0.0005(1)		0.0013(2)	
R(%)		5.5		14.4	

FTs of $k^3\chi(k)$ shows large differences in the nearest-neighbor peak magnitude with Ga concentration, as demonstrated in Fig. 5. Similar differences have been previously reported.[29] For the present data, the 1.9 at. % Ga sample shows the highest amplitude for the nearest-neighbor scatterer from both edges.

In addition to the overall loss of amplitude with change Ga concentration, both the 4.3 at. % Ga and the 7.0 at. % Ga data show evidence of Pu-Pu scattering corresponding to a pair distance of about 3.8 Å, a distance that is not consistent with the *fcc* phase. The scattering associated with this distance is visible in Fig. 5(a) as a distinct peak just to the right of the main peak for the 4.3 at. % Ga and 7.0 at. % Ga data, whereas the peak is washed out in the 1.9 at. % Ga data. Such a peak has been previously observed, both in EXAFS data[28,29] and in recent PDF data.[33] Here, as in Ref. 29, the peak is also clearly correlated with the loss of EXAFS amplitude in the main peak. Concurrently, extra amplitude in the EXAFS spectrum is present between 1 and 2 Å for these samples. A fit to Pu-O scattering has been considered, but if the amplitude is due to Pu-O, several distances must be involved between 1.7 Å and 2.3 Å. The complexity of such a fit renders

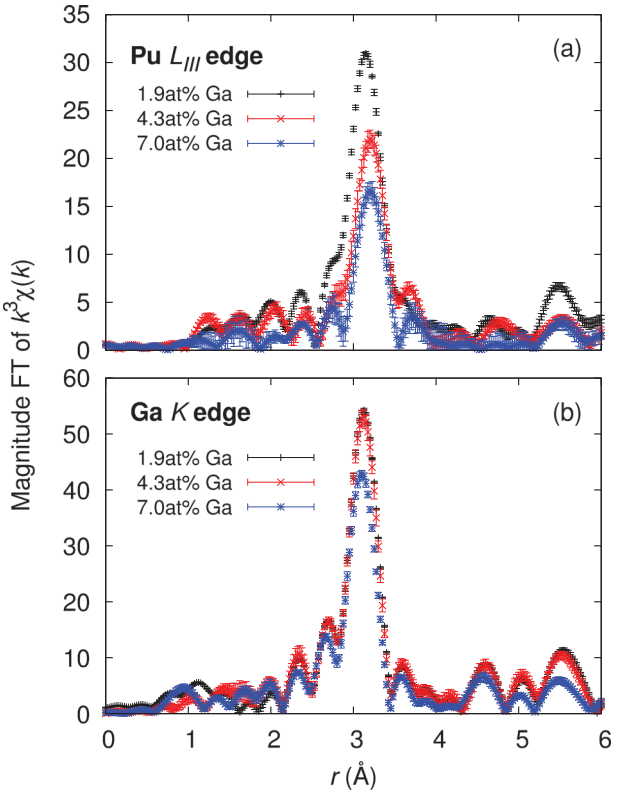

FIG. 5. EXAFS magnitudes at low temperature for δ-Pu samples with Ga concentrations of 1.9 at. % (30 K), 4.3 at. % (5 K), and 7.0 at. % (30 K) from the (a) Pu L_3 edge and (b) the Ga K edge. Transforms are from 2.5 to 14.0 Å^{-1} for the Pu L_3-edge data, and from 2.5 to 13.9 Å^{-1} for the Ga K-edge data, each Gaussian narrowed by 0.3 Å^{-1}. All samples had been at RT directly before measurement.

the results unreliable, and so we only consider the 3.8 Å Pu-Pu peak here. Results of such fits are reported in Table II, which includes results on the 1.9 at. % Ga sample using this methodology. Here, we label the impurity as a "σ phase," consistent with the original labeling.[29] Assuming the 3.8 Å peak corresponds to a phase with 8 Pu-Pu neighbors near this distance (as occurs for both the *bcc*-like phase and PuO_2), this second phase accounts for the loss of amplitude as measured by the reduced S_0^2, giving a more reasonable effective total $S_0^2 \approx 0.9$. These results are qualitatively consistent with the original measurements; however, the original measurements indicate the "σ phase" only exists within the Ga concentration range of 1.70–3.35 at. % Ga. The present fit results firmly indicate a 3.8 Å pair for the 4.3 at. % Ga data (18% ± 7% of the sample assuming a *bcc*-like "σ phase," see Table II). In addition, the visible presence of the peak in the 7.0 at. % Ga data is evidence for the existence of this pair for this Ga concentration, although the fit result is inconclusive (5 ± 5%), although it is important to note that there is no evidence of a similar peak from the Ga K edge; the peak to the right of the main peak is fit well using only the Pu-Ga scattering at ~3.1 Å. These results, therefore, indicate the possible presence of the "σ phase" over a broader Ga concentration range than originally observed.

One argument for the apparently strong effect of Ga on the local structure in δ-Pu is that the effect of the distortions around the Ga impurities is amplified due to the 12 nearest-neighbor Pu atoms. For instance, if each Ga-Pu distorts 12 Pu-Pu pairs in the second coordination shell by 0.05 Å, one expects to obtain a static contribution to the Pu-Pu Debye-Waller factor, $\sigma^2_{stat} = 0.0025\,\text{Å}^2 \times 4.3\% \times 12 = 0.0013\,\text{Å}^2$. In fact, this value is in good agreement with the data: By fitting the temperature dependence of the measured σ^2 results with the correlated-Debye model, we obtain $\sigma^2_{stat} = 0.0010 \pm 0.0002\,\text{Å}^2$.

Therefore, at least for the data presented here, the local structure of δ-Pu can be described as well ordered, except for Ga-induced distortions in the second coordination sphere around each Ga impurity and possibly a Ga-induced second *bcc*-like phase in some samples.

The effect of radiation damage on the 1.9 at. % Ga sample as a function of storage time measured in α-decays per atom is included in Fig. 3 (inverted triangles). The damage accumulation for δ-Pu material stored at room temperature (T_S = RT) is clearly much slower than in the other measured materials. As demonstrated previously from both electrical resistivity[34,35] and magnetic susceptibility measurements,[14] most of the accumulated damage can be annealed out below room temperature.

It is important to note that the 1.9 at. % Ga sample, while the best ordered of the three available δ-Pu samples, is also susceptible to the martensitic, partial $\delta - \alpha'$ transition as it is cooled through approximately 140 K.[36] Any so-called "damage" observed for this sample could actually be due to this transition; therefore, what little damage shown in Fig. 3 for that sample could be considered as an upper limit. However, signatures of the α' phase, such as scattering due to Pu-Pu pairs at 2.62 Å or 3.39 Å (Ref. 37) were not observed.

TABLE II. Fit results to data from Fig. 5. Fit range is between 2.5 and 4.1 Å. Pu-Ga pair amplitudes are fixed by the nominal Ga concentration, and their pair distances are determined from Ga K-edge fits and held fixed here. See Table I caption for further details.

	1.9 at. % Ga			4.3 at. % Ga			7.0 at. % Ga		
	σ^2(Å^2)	R(Å)	A	σ^2(Å^2)	R(Å)	A	σ^2(Å^2)	R(Å)	A
Pu-Pu	0.0029(1)	3.267(1)	10.1	0.0036(2)	3.257(2)	7.79	0.0064(3)	3.250(3)	10.4
Pu-Ga	0.006(5)	3.134	0.2	0.003(2)	3.127	0.35	0.004(1)	3.120	0.79
Pu-Pu("σ phase")	0.004(3)	3.85(1)	0.86	0.002(1)	3.799(5)	1.56	0.001(1)	3.79(1)	0.40
ΔE_0		2.3(4)			−6.5(6)			−6.4(5)	
$A_1/12$ (*fcc*)		0.86(3)			0.68(5)			0.94(6)	
$A_2/8$ ("σ phase")		0.1(1)			0.18(7)			0.05(5)	
R (%)		2.4			4.5			6.6	

In order to establish the actual local structure effect of damage production and to separate the effect of annealing, a sample of δ-Pu was held below 5 K (with <2 min transient to 32 K just prior to the final measurement) at SSRL for a period of two months (storage temperature $T_S < 32$ K). The 4.3 at. % Ga sample was chosen for this experiment to avoid the complications of partial α' formation, and also for better comparisons to a previous annealing study[14] which used this concentration. As can be seen in Fig. 6, significant damage was produced, above 40% damage after only 6.5×10^{-6} α-decays per atom, exceeding the observed damage production rate for any of the $T_S =$ RT samples.

The EXAFS were collected as a function of heating after two months of cryogenic aging in order to look for annealing steps similar to those observed in the resistivity and susceptibility measurements. Ideally, one would follow the previous work[14,34,35] and heat a sample to some temperature, then cool it back to some low temperature (e.g., 5 K) and take a new measurement. This method would eliminate the thermal broadening differences that occur for measurements at different temperatures. This method could not be employed due to experimental limitations. Also, unfortunately, an equipment malfunction prevented the cryostat from controlling temperature between about 50 K and 135 K, and consequently no useful data could be collected in this temperature range.

The damage fraction in the sample could nevertheless be extracted as a function of temperature using the fact that the local structure broadening follows the correlated-Debye model well,[30] and so damage fractions were obtained by constraining the 3.27 Å Pu-Pu scattering peak to have a $\sigma^2(T)$ that corresponds to the correlated-Debye model fits carried out when the sample was freshly annealed. This procedure is responsible for larger estimated errors, especially near room temperature. Another complication is the aforementioned *bcc*-like scattering at a Pu-Pu pair distance of 3.8 Å. As can be seen in Fig. 6(a), this peak appears to be largely unaffected as damage accumulates in the rest of the crystal, and so damage estimates hold the fraction of this peak fixed as the damage is removed with rising temperature, although its σ^2 is allowed to vary.

The damage fraction of the $T_S < 32$ K sample after two months is shown in Fig. 7(a) as a function of temperature on heating. As can be seen, more than 40% of the atoms are in a damaged environment until a temperature between 50 and 135 K. By 135 K, any remaining damage is below the detection limit. A final data set was collected after cooling back to 5 K to verify that all the damage was removed. Fig. 7(b) shows the change in the damage fraction from the low-temperature value, $\Delta F_d(T) - F_d(5\,\mathrm{K})$, normalized by $F_d(5\,\mathrm{K})$, as a comparable variable to that used in the isochronal annealing studies, where the damage fraction change ΔF_d is either given by the fractional resistivity change[35] or the fractional magnetic susceptibility change.[14] Although the local structure data are sparse in

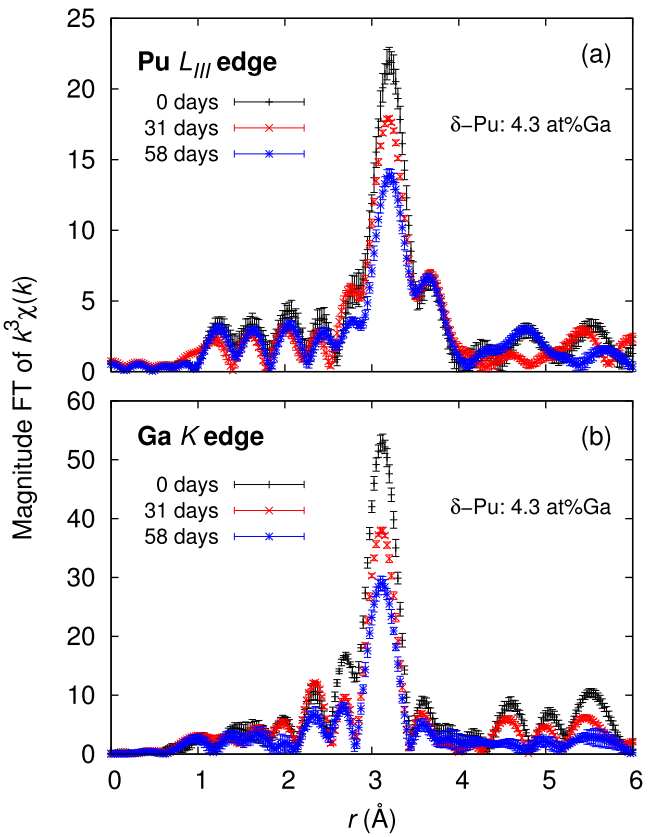

FIG. 6. EXAFS magnitudes for the δ-Pu: 4.3 at. % Ga sample at low temperature from (a) the Pu L_3 edge and (b) the Ga K edge for sample ages since last anneal of 0.0 α-decays per atom at 30 K, 3.2×10^{-6} α-decays per atom at 5.5 K, and 6.5×10^{-6} α-decays per atom at 5.0 K.

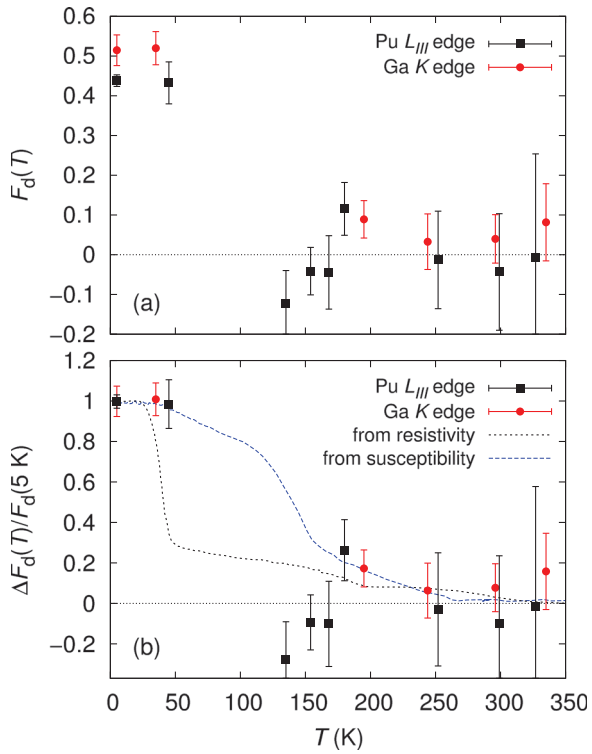

FIG. 7. Local structure damage results for cold-stored δ-Pu sample. (a) Total damage fraction as measured by EXAFS as a function of temperature on warming after stored for 2 months below 32 K. (b) Same data as in (a) replotted as the change in measured damage from $T = 5$ K, normalized by the measured damage at 5 K. Note that unphysical $F_d < 0$ results can occur if the EXAFS amplitude actually increases with time. The estimated errors indicate such results are consistent with no developed damage. The EXAFS data are also compared to previous resistivity[35] and susceptibility[14] data, similarly normalized taking $F_d = \rho$ and $F_d = \chi$, respectively.

the region of the biggest changes, clear differences and similarities exist. Specifically, damage accumulates substantially at low temperature, and all the measurements agree that most of the damage is removed after about 150 K. At low T, the local structure results seem to follow the susceptibility data, showing little damage reduction at or below 45 K. Interestingly, the local structure indication that all measurable damage is removed by 135 K is *not* consistent with the susceptibility data, but is consistent with the resistivity data. However, it is known that the impurity (in this case, Ga) concentration can affect the exact position of the primary annealing step,[34] and the resistivity sample has a somewhat lower Ga concentration (3.3 at. % Ga) than the local structure sample (4.3 at. % Ga). More data in the critical temperature range between 50 and 135 K, possibly as a function of Ga concentration, are needed to elucidate these issues, but it does appear that the susceptibility measurement is more sensitive to certain defects than EXAFS or resistivity.

IV. DISCUSSION

These data, while far from allowing for a complete microscopic picture of self-irradiation damage in Pu intermetallics, do allow for a discussion of radiation damage effects as they relate to the vibrational and chemical makeup of a given material and the role of temperature. The most striking result is the amount of damage that can accumulate in a material if the temperature is kept sufficiently low, with nearly half of the Pu atoms strongly displaced, either as Frenkel defects or from local distortions, after only 0.00062% of the Pu atoms have undergone α-decay. In other words, about 75 000 Pu atoms are strongly distorted or displaced per α-decay, corresponding to a volume of 1850 nm^3. This volume is about a factor of two larger than the approximate volume encompassed within a damage cascade: A U recoil in δ-Pu travels about 12 nm,[3] which, if taken as the diameter of a sphere, corresponds to a volume of 904 nm^3 (we ignore the much smaller effect of the α particle in this discussion). It appears that at least every atom within a damage cascade is displaced, a conclusion that was also reached in the work on the $PuCoGa_5$ superconductor.[16] Moreover, the range of distortions around each defect likely extends to at least the third neighbor, creating a deep, distorted skin around the damage cascade. This situation is, indeed, similar to the case even for the smaller defects measured around each Ga impurity site, as first noted by Cox *et al.*,[25] which showed clear distortions in the second Ga-Pu shell, and possibly the third.

It is interesting to compare this volume with that obtained from previous magnetic susceptibility measures of the cascade volume,[14] which are an order of magnitude larger at 13 600 nm^3. It was conjectured that the volume derived from susceptibility could be enhanced as the result of extended features, such as strain fields around a defect. The present data support that interpretation, since even using a very local probe that is exploring only the first 4 Å around each Pu and Ga atom, we obtain a cascade volume larger than given by the U recoil path itself. Given the large volume per decay, the effect of such strain fields would quickly dominate the entire sample. For example, the local effects as measured by EXAFS indicate that about half the sample is affected after only two months. With the enhanced volume detectable by susceptibility, nearly the entire sample should experience some effect of the damage after this much time has passed.

Historically, the amount of damage caused by self-irradiation has been equated to the number of Frenkel defect pairs formed (interstitial + vacancy = 1 pair). Within the standard Kinchin and Pease model,[2] each lattice site has an associated displacement energy, E_d. This displacement energy is the energy required to completely displace an atom from its lattice site, similarly to an escape velocity. It does not, however, say anything about whether the vacancy it left behind gets filled somehow, such as from a different displaced atom. In any case, the simplest way to estimate E_d is from the material's melting temperature, where $E_d \simeq 175 k_B T_m$. Given δ-Pu's $T_m = 913$ K, $E_d \simeq 14$ eV. Following the discussion made by Wolfer,[12] about half of all collisions impart this much energy, and so the number of interstitial defects should be about 2300 (about 25% of the 86 keV U recoil energy is lost to electrons). All modern calculations include the physics within a modified version of this simple argument.[1]

The melting temperatures of most of the measured compounds are unknown (although greater than 1200 K). As an alternative, one can consider the Lindemann criterion for melting to obtain an estimate of T_m from a measure of the Debye temperature

$$T_m = \frac{f^2 r^2 \mu_r}{9\hbar} k_B \Theta_D^2.$$

This version of the formulation accounts for differing species for a given atomic pair, and was originally derived for mixed and ionic crystals.[38] From this expression, it is clear that the higher the Debye temperature (the stiffer the bond), the higher the T_m, and the lower the number of defects produced per α-decay. The results in Fig. 3 clearly do not follow this trend, however, at least for the T_S = RT results: δ-Pu, which has the lowest Θ_D (and the lowest T_m) shows the slowest damage rate of the measured samples. This result merely underscores the importance of lattice relaxation after defect production.

Lattice relaxation is known to rapidly fill most of these defects, as has been seen in molecular dynamics calculations.[3,4] The rate and the number of this defect-filling are strongly dependent on temperature,[4] and the relative strength of the bonds. We, therefore, have two competing effects, each of which depends on the bond strength: defect production and defect annealing. For samples stored at RT, annealing is actually the dominant effect: the molecular dynamics calculations show about 2000 defects formed for a 20 keV recoil at 300 K after 400 ps, but the number at 180 K is diverging beyond 10^6 after less than 30 ps.[4]

Indeed, a very rough correlation exists in the present data between the amount of damage that accumulates at RT and the vibrational properties of the material, since the Debye temperature of δ-Pu is the lowest of the measured samples (about 100 K (Ref. 30)), while the amount of damage annealed out is clearly large as observed from the

contrast between the $T_S < 32$ K and the $T_S = $ RT data, and the slow rate of damage accumulation for $T_S = $ RT, especially from the Ga edge. However, this comparison does not hold strictly. For instance, the damage accumulation for the $PuGa_3$ sample data is very similar to those from δ-Pu with $T_S < 32$ K, even though $\Theta_D = 275$ K for $PuGa_3$ (Ref. 8) is much larger than that of δ-Pu. Moreover, the local vibrational properties for, say, the Pu-Ga pair in $PuCoGa_5$ compared to the Pu-Al pair in $PuAl_2$, also do not correlate strongly with the damage annealing: Θ_{cD} is about 330 K for Pu-Ga in $PuCoGa_5$,[16] while it is about 370 K for Pu-Al in $PuAl_2$ from the data presented here, despite the clearly larger damage accumulated in $PuCoGa_5$. To further contrast this result, Θ_{cD} for Pu-Ga in $PuGa_3$ is estimated to be 211 K.

A simple rule equating melting with defect production and annealing is, therefore, not good enough to make even qualitative predictions about a material. It is, of course, known that details of the lattice matter, as do the individual bonding sympathies of a particular atomic species or pair of species.[39,40] The present materials were chosen, in part, because the metallic bonding that occurs in these materials is largely not directional; that is, the crystal structures are mainly determined by packing requirements rather than bonding requirements. This situation is in contrast to, say, an oxide, where a local 8-fold coordination predominates. However, clear differences occur between the local structures around different elements within the same sample. For instance, the Pu_2PtGa_8 data in Fig. 2 show strikingly different damage from the Pu L_3-edge data compared to the Ga K-edge data. Between 171 and 284 days since the sample was initially synthesized, there is almost no difference in the EXAFS amplitude, yet the amplitude falls by about 40% from the Ga edge data.

Within this picture, the Ga edge data for the $T_S = $ RT δ-Pu sample are particularly intriguing. Of all the samples at all the measured edges, it is the only one that has an EXAFS spectrum consistent with no damage developing. However, this stabilization is clearly due to a fast annealing at RT, since the damage production rate around Ga for $T_S < 32$ K is actually *larger* for Ga than Pu. Both the larger damage for $T_S < 32$ K and the larger annealing at RT are inconsistent with the concept of a displacement energy and its relation to the vibrational properties, since the Ga-Pu pairs are known to be stiffer[30] than the Pu-Pu pairs, which, using the Lindemann criterion above, implies a smaller E_d and easier annealing. On the other hand, it is interesting to note that the $T_S = $ RT data for δ-Pu (1.9 at. % Ga) are nearly identical to those for $PuGa_3$. The particular bonding characteristics of Ga clearly play the more important role, emphasizing that gallium's role as a *fcc* stabilizer in Pu also extends to damage effects.

Given gallium's role as a network stabilizer and potentially also as a damage reducer, it is interesting to consider its role in possibly removing damage from the "σ phase" (the $\sim$3.8 Å peak in Fig. 6(a)). The fact that this peak maintains its amplitude while the rest of the local structure is damaged with time is a good evidence of the existence of a second phase, and apparently one that can reform its local structure as do highly directional bonded materials such as PuO_2.[39–41] However, this local self-healing maintains even for a sample stored below 32 K, and it is unknown to the present authors whether low-temperature annealing studies have been performed on PuO_2 or similar materials in the past,[42] although low-temperature studies have shown greatly accelerated damage production from increasing lattice parameters in Cm_2O_3, and that the damage is essentially removed by 300 °C.[43]

The measured changes in the damage fraction with time (Fig. 3) can be considered in terms of an equilibrium between damage production and annealing. The following model is a gross simplification given the different kinds of defects (vacancies, interstitials, possible local phase formation, surface to volume effects that are obviously shape dependent, etc.), so it is presented as a semi-quantitative model that describes the main features of the data. Assuming the number of ordered lattice sites, N_O, decreases due to radiation damage as $dN_O = -K_r N_O dn$, where n is the cumulative number of α-decays per atom (measuring time in terms of the total dose per atom), the rate constant $K_r = n_d$, n_d is the number of distorted atoms per decay, and the total number of distorted atoms, N_d, decreases due to annealing as $dN_d = -K_a N_d dn$, one obtains

$$dF_d = [K_r + (K_r + K)F_d]dn, \tag{1}$$

where K_a the distorted-atom annealing rate. The result of this formula is shown as model "m1" in Figs. 3 and 8 with no annealing ($K_a = 0$) and $n_d = 90\,000$ distorted atoms per decay. The $T_S = $ RT data for both δ-Pu and $PuGa_3$ then are consistent with $K_a = 4.5 \times 10^5$ per decay (model "m2"). An activated form for $K_a = K_0 \exp(-E_a/k_B T)$ likely applies; however, more data at intermediate T_S would be required to determine K_0 and E_a.

Although a single annealing rate, K_a, describes the data for δ-Pu and $PuGa_3$ reasonably well, a second annealing rate is necessary to describe the $PuCoGa_5$ and $PuAl_2$ data, where F_d increases slowly after a quick initial jump, as opposed to a nearly flat F_d with dose after the initial rise. These data can be

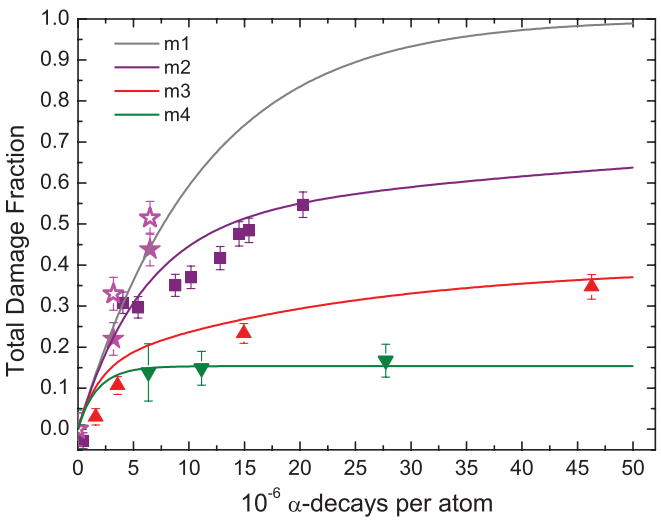

FIG. 8. Total damage fraction F_d calculated from the simple equilibrium models described in the text. Each model uses the same damage production rate of 90 000 distorted atoms per decay. Model "m1" has no annealing, and the annealing rate increases from "m2" through "m4." Data shown follow legend from Fig. 3, with δ-Pu for $T_S < 32$ K (stars), $PuCoGa_5$ (filled squares), $PuAl_2$ (triangles), and δ-Pu for $T_S = $ RT (inverted triangles).

roughly modeled assuming numbers of two kinds of defects, N_1 and N_2, each with their own annealing rates, K_1 and K_2. Note that each type of defect, for instance, those due to local phase formation, likely has its own annealing rate, and it is not possible to know which type of defect corresponds to which annealing rate. However, if one considers a surface-to-volume effect with N_1 describing the defects within the core of the cascade and N_2 the defects on the edges, one expects $N_1 > N_2$ (surface to volume) and $K_1 < K_2$. In this model, the initial damage would be created with $N_1 = cN_2$, and then the defects would anneal at the prescribed rate. The $PuCoGa_5$ data can be described (model "m3") with $c = 5$, $K_1 = 9 \times 10^5$ per decay, and $K_2 = 5 \times 10^3$ per decay, and the $PuAl_2$ data can be similarly described model ("m4") with $c = 5$, $K_1 = 4.5 \times 10^5$ per decay, and $K_2 = 3 \times 10^4$ per decay (Fig. 8). Although the data are described using only two annealing rates, more are likely present: at least 5 annealing steps are observed in the isochronal annealing curves.[14,34,35]

V. CONCLUSION

The EXAFS technique has provided a sub-Ångström-scale measure of the local distortions generated by self-irradiation in various plutonium intermetallic compounds and in the *fcc* phase of elemental Pu, providing a quantitative measure of the fraction of damaged material. Although damage is observed to develop at similar rates for all the measured samples at low total doses (short times), annealing effects quickly dominate. Such effects dominate especially quickly in, for instance, δ-Pu, where what little damage can develop is saturated after only two months in the measured sample. By storing one δ-Pu sample below 32 K for two months, the effect of annealing was removed and very substantial amounts of damage developed. While differences in damage production and annealing between various compounds can be very roughly understood in terms of their vibrational properties, the dominant property governing damage production and annealing appears to be unique to the particular bonds within the compound. This latter result implies that billiard-ball-type methods[1,2] are clearly inadequate for calculating radiation damage effects in plutonium compounds. For instance, the importance of the bonding details is exemplified by Ga *K*-edge data on δ-Pu and some intermetallic compounds that emphasize gallium's role not only as a network stabilizer but also as a potential damage-reducer. Moreover, the annealing data and the differences in the local environment around different atomic species indicate that the sample history is very important for eventually predicting damage effects for real materials. Finally, we note that annealing plays a very large role in determining the damage in a given material, apparently even for materials with relatively average vibrational properties. Careful isochronal annealing studies should be carried out on any material likely to undergo radiation damage.

ACKNOWLEDGMENTS

We gratefully acknowledge several conversations with Steve Valone. Work at Lawrence Berkeley National Laboratory was supported by the Director, Office of Science (OS), Office of Basic Energy Sciences (OBES), Chemical Sciences, Geosciences, and Biosciences Division of the U.S. Department of Energy (DOE) under Contract No. DE-AC02-05CH11231. Work at Los Alamos National Laboratory (LANL) was performed under the auspices of the U.S. DOE, OS, Materials Science and Engineering Division, and the LANL LDRD Program. Work at Lawrence Livermore National Laboratory work was performed under the auspices of the U.S. DOE under Contract No. DE-AC52-07NA27344. X-ray absorption data were collected at the Stanford Synchrotron Radiation Lightsource, a national user facility operated by Stanford University on behalf of the DOE, OBES.

[1]M. J. Norgett, M. T. Robinson, and I. M. Torrens, Nucl. Eng. Des. **33**, 50 (1975).
[2]G. H. Kinchin and R. S. Pease, Rep. Prog. Phys. **18**, 1 (1955).
[3]T. Diaz de la Rubia, M. J. Caturla, E. A. Alonso, N. Soneda, and M. D. Johnson, Radiat. Eff. Defects Solids **148**, 95 (1999).
[4]A. Kubota, W. G. Wolfer, S. M. Valone, and M. I. Baskes, J. Comput.-Aided Mater. Des. **14**, 367 (2007).
[5]C. H. Booth, Y. Jiang, D. L. Wang, J. N. Mitchell, P. H. Tobash, E. D. Bauer, M. A. Wall, P. G. Allen, D. Sokaras, D. Nordlund, T.-C. Weng, M. A. Torrez, and J. L. Sarrao, Proc. Natl. Acad. Sci. U.S.A. **109**, 10205 (2012).
[6]Q. Yin, A. Kutepov, K. Haule, G. Kotliar, S. Y. Savrasov, and W. E. Pickett, Phys. Rev. B **84**, 195111 (2011).
[7]J. L. Smith and Z. Fisk, J. Appl. Phys. **53**, 7883 (1982).
[8]P. Boulet, E. Colineau, F. Wastin, P. Javorsky, J. C. Griveau, J. Rebizant, G. R. Stewart, and E. D. Bauer, Phys. Rev. B **72**, 064438 (2005), Θ_D determined by fitting data above antiferromagnetic transition.
[9]J. L. Sarrao, L. A. Morales, J. D. Thompson, B. L. Scott, G. R. Stewart, F. Wastin, J. Rebizant, P. Boulet, E. Colineau, and G. H. Lander, Nature (London) **420**, 297 (2002).
[10]E. D. Bauer, M. M. Altarawneh, P. H. Tobash, K. Gofryk, O. E. Ayala-Valenzuela, J. N. Mitchell, R. D. McDonald, C. H. Mielke, F. Ronning, J.-C. Griveau, E. Colineau, R. Eloirdi, R. Caciuffo, B. L. Scott, O. Janka, S. M. Kauzlarich, and J. D. Thompson, J. Phys.: Condens. Matter **24**, 052206 (2012).
[11]H. B. Rhee, F. Ronning, J.-X. Zhu, E. D. B. J. N. Mitchell, P. H. Tobash, B. L. Scott, J. D. Thompson, Y. Jiang, C. H. Booth, and W. E. Pickett, Phys. Rev. B **86**, 115137 (2012).
[12]W. G. Wolfer, Los Alamos Sci. **26**, 274 (2000).
[13]I. Farnan, H. Cho, and W. J. Weber, Nature (London) **445**, 190 (2007).
[14]S. K. McCall, M. J. Fluss, B. W. Chung, M. W. McElfresh, D. D. Jackson, and G. F. Chapline, Proc. Natl. Acad. Sci. U.S.A. **103**, 17179 (2006).
[15]C. H. Booth, M. Daniel, R. E. Wilson, E. D. Bauer, J. N. Mitchell, N. O. Moreno, L. A. Morales, J. L. Sarrao, and P. G. Allen, J. Alloys Compd. **444**, 119 (2007).
[16]C. H. Booth, E. D. Bauer, M. Daniel, R. E. Wilson, J. N. Mitchell, L. A. Morales, J. L. Sarrao, and P. G. Allen, Phys. Rev. B **76**, 064530 (2007).
[17]E. D. Bauer, P. H. Tobash, J. N. Mitchell, and J. L. Sarrao, Philos. Mag. **92**, 2466 (2012).
[18]C. H. Booth and F. Bridges, Phys. Scr. **T115**, 202 (2005).
[19]G. G. Li, F. Bridges, and C. H. Booth, Phys. Rev. B **52**, 6332 (1995).
[20]RSXAP Analysis Package, see http://lise.lbl.gov/RSXAP/ (2012).
[21]T. M. Hayes and J. B. Boyce, "Extended x-ray absorption fine-structure spectroscopy," in *Solid State Physics*, edited by H. Ehrenreich, F. Seitz, and D. Turnbull (Academic, New York, 1982), Vol. 37, p. 173.
[22]A. L. Ankudinov, B. Ravel, J. J. Rehr, and S. D. Conradson, Phys. Rev. B **58**, 7565 (1998).
[23]W. H. Zachariasen, Acta Crystallogr. **2**, 388 (1949).
[24]C. H. Booth and Y. Hu, in *Proceedings of X-Ray Absorption Fine Structure – XAFS14: 14th International Conference, 26–31 July, 2009* [J. Phys.: Conf. Ser. **190**, 012028 (2009)].
[25]L. E. Cox, R. Martinez, J. H. Nickel, S. D. Conradson, and P. G. Allen, Phys. Rev. B **51**, 751 (1995).
[26]Ph. Faure, B. Deslandes, D. Bazin, C. Tailland, R. Doukhan, J. M. Fournier, and A. Falanga, J. Alloys Compd. **244**, 131 (1996).
[27]N. Richard, Ph. Faure, P. Rofidal, J. L. Truffier, and D. Bazin, J. Alloys Compd. **271–273**, 879 (1998).

[28]S. D. Conradson, Appl. Specrosc. **52**, 252A (1998).
[29]S. D. Conradson, Los Alamos Sci. **26**, 356 (2000).
[30]P. G. Allen, A. L. Henderson, E. R. Sylwester, P. E. A. Turchi, T. H. Shen, G. F. Gallegos, and C. H. Booth, Phys. Rev. B **65**, 214107 (2002).
[31]G. Beni and P. M. Platzman, Phys. Rev. B **14**, 1514 (1976).
[32]E. D. Crozier, J. J. Rehr, and R. Ingalls, in *X-Ray Absorption: Principles, Applications, Techniques of EXAFS, SEXAFS, XANES*, edited by D. Konigsberger and R. Prins (Wiley, New York, 1988), p. 373.
[33]C. Platteau, P. Bruckel, B. Ravat, and F. Delaunay, J. Nucl. Mater. **385**, 108 (2009).
[34]D. A. Wigley, Proc. R. Soc. London, Ser. A **284**, 344 (1965).
[35]M. J. Fluss, B. D. Wirth, M. Wall, T. E. Felter, M. J. Caturla, A. Kubota, and T. Diaz de la Rubia, J. Alloys Compd. **368**, 62 (2004).
[36]K. J. M. Blobaum, C. R. Krenn, M. A. Wall, T. B. Massalski, and A. J. Schwartz, Acta Mater. **54**, 4001 (2006).
[37]E. J. Nelson, K. J. M. Blobaum, M. A. Wall, P. G. Allen, A. J. Schwartz, and C. H. Booth, Phys. Rev. B **67**, 224206 (2003).
[38]S. Rabinovich, D. Berrebi, and A. Voronel, J. Phys.: Condens. Matter **1**, 6881 (1989).
[39]K. Trachenko, J. Phys.: Condens. Matter **16**, R1491 (2004).
[40]K. Trachenko, J. M. Pruneda, E. Artacho, and M. T. Dove, Phys. Rev. B **71**, 184104 (2005).
[41]N. J. Hess, W. J. Weber, and S. D. Conradson, J. Alloys Compd. **271–273**, 240 (1998).
[42]M. Noe and J. Fuger, Inorg. Nucl. Chem. Lett. **10**, 7 (1974).
[43]M. Noe, J. Fuger, and G. Duyckaerts, Inorg. Nucl. Chem. Lett. **6**, 111 (1970).